

On Narrow-Band Representation of Ocean Waves

2. Simulations

M. AZIZ TAYFUN

Civil Engineering Department, College of Engineering and Petroleum, Kuwait University

In paper 1 (Tayfun, this issue) we derived two narrow-band type representations for nonlinear waves and obtained theoretical expressions for the key statistics of the corresponding surface elevations, namely, the variance, skewness, and kurtosis. The nature of these statistics and the underlying probability structure were examined qualitatively with particular emphasis on the effects of the spectrum bandwidth. In this paper we explore the reliability of these results quantitatively. Proceeding via the Monte Carlo approach and finite Fourier transform techniques, we generate extensive samples of surface time history with preassigned spectral and statistical properties. Each sample is synthesized from a systematic superposition of the first-order linear field and the second-order corrections, consisting of shortwave and long-wave modulations, respectively. This approach enables us to demonstrate explicitly the individual as well as combined effects of second-order nonlinearities on the probability distribution and statistics of the surface elevation. In the final analysis we find that the simulated results compare favorably with the theoretical predictions and confirm the validity of various qualitative arguments put forward in paper 1.

1. INTRODUCTION

In the companion paper [Tayfun, this issue], hereinafter referred to as paper 1, we reviewed the effects of second-order nonlinearities on the spectrum and statistical properties of unidirectional waves in deep water. Under the usual assumption that such a wave field is weakly nonlinear, the surface elevation with respect to the mean sea level is described in the form $\eta = \eta_1 + \eta_2$, where η_1 and η_2 denote the first-order linear field and the second-order nonresonant interactions induced by η_1 , respectively. The latter is decomposed further into two components, $\eta_{2,s}$ and $\eta_{2,l}$, representing the shortwave and long-wave modulations. In essence, $\eta_{2,s}$ imposes a vertical asymmetry on η_1 , and $\eta_{2,l}$ causes relatively long period fluctuations in the mean sea level.

From a practical viewpoint it appears that both modulations can have profound effects on the observation, forecast, and interpretation of principal wave characteristics and on the dynamic behavior of fixed or floating marine structures. Therefore a theoretical understanding of the effects of $\eta_{2,s}$ and $\eta_{2,l}$ on the statistical distribution of sea surface elevations is of considerable interest. To achieve this objective in the most general case is difficult because of the mathematics involved. Nonetheless, in the special case when the frequency spectrum of the surface is narrow banded, one can make some progress toward a relatively simple theory. This line of thought eventually led us to the derivation of two narrow-band representations of η .

The frequency spectrum S (in particular, its bandwidth ν) plays a central role in determining the surface properties. This role becomes still more evident in the two models of paper 1, which approximate the "exact" form of η to $O(\nu^0)$ and $O(\nu)$, respectively. The principal advantage of these models is that they are relatively simple to deal with, so that we can determine the effects of $\eta_{2,s}$ and $\eta_{2,l}$ on the physical structure and probability density of η quite easily. In particular, the probability density of η has the usual form of the Gram-Charlier series [Longuet-Higgins, 1963], but the key statistical parameters required in this form, namely, the variance σ_η , skewness

λ_3 , and kurtosis λ_4 , are given in terms of simpler expressions. To be specific, we have to $O(\nu)$

$$\sigma_\eta = m_0^{1/2}(1 + \frac{1}{2}\alpha^2)^{1/2} \quad (1)$$

$$\lambda_3 = \frac{3}{2^{1/2}} \alpha(1 + \frac{1}{2}\alpha^2)^{-3/2}(1 - \gamma) \quad (2)$$

$$\lambda_4 = 6\alpha^2(1 + \frac{1}{2}\alpha^2)^{-2}(1 - 2\gamma) \quad (3)$$

where γ is $O(\nu)$ and is related to the spectral shape. Moreover, $0 \leq \gamma \leq \sqrt{2\nu}$, so that λ_3 and λ_4 given by (2) and (3) satisfy the following inequalities:

$$\lambda_{3,l} \leq \lambda_3 \leq \lambda_{3,u} \quad (4)$$

$$\lambda_{4,l} \leq \lambda_4 \leq \lambda_{4,u} \quad (5)$$

where

$$\lambda_{3,l} = \frac{3}{2^{1/2}} \alpha(1 + \frac{1}{2}\alpha^2)^{-3/2}(1 - \sqrt{2\nu}) \quad (6)$$

$$\lambda_{4,l} = 6\alpha^2(1 + \frac{1}{2}\alpha^2)^{-2}(1 - 2\sqrt{2\nu}) \quad (7)$$

and the upper bounds

$$\lambda_{3,u} = \frac{3}{2^{1/2}} \alpha(1 + \frac{1}{2}\alpha^2)^{-3/2} \quad (8)$$

$$\lambda_{4,u} = 6\alpha^2(1 + \frac{1}{2}\alpha^2)^{-2} \quad (9)$$

represent the limiting forms of λ_3 and λ_4 when $\nu \rightarrow 0$. These limits and (1) are also appropriate to and follow from the simpler model, which is $O(\nu^0)$ and does not take into account any contribution from $\eta_{2,l}$. The parameter α is a measure of wave steepness. We define it in the form $\alpha = \langle k \rangle (2m_0)^{1/2}$, where $m_0^{1/2}$ denotes the first-order variance and $\langle k \rangle$ denotes the spectral mean wave number. Oceanic observations suggest that $0 < \alpha < 0.2$ [Huang et al., 1981], although this range is likely to be somewhat biased against extreme seas.

Both $\eta_{2,s}$ and $\eta_{2,l}$ are $O(\alpha)$, but they have exactly opposite effects on λ_3 and λ_4 . Specifically, $\eta_{2,s}$ tends to increase λ_3 and λ_4 , whereas $\eta_{2,l}$ reduces them both. However, this happens in a manner quite dependent on the spectrum bandwidth because $\eta_{2,l}$ is also $O(\nu)$. This simply means that when the spectrum has a wide bandwidth so that ν is $O(1)$, the effect of $\eta_{2,l}$ is

Copyright 1986 by the American Geophysical Union.

Paper number 6C0110.
0148-0227/86/006C-0110\$05.00

comparable to and tends to neutralize that of $\eta_{2,s}$. In this case we suspect that the skewness and excess associated with the surface density will both be slight. Conversely, when the spectrum bandwidth is very narrow so that $v^2 \ll 1$, the effect of $\eta_{2,i}$ is essentially negligible, and so the surface density corresponding to the same steepness must display a more pronounced positive skewness and larger excess at the mode.

Because all the preceding qualitative arguments and theoretical results follow from the narrow-band approximations, their validity and quantitative accuracy need to be verified with respect to the predictions implied by the exact form of η . Provided that such a verification proves favorable, one would ultimately hope to relate the theoretical results to actual observations. Therefore our immediate goal is to explore the quantitative reliability of the statistics σ_η , λ_3 and λ_4 by comparing them with those to be derived from the exact form of η for various values of α and v . Further, we aim to examine the probability densities of $\eta_{2,s}$ and $\eta_{2,i}$ and their individual and combined effects on the distribution of surface elevations as an explicit demonstration of the qualitative arguments put forward in paper 1. We will achieve these objectives most conveniently by simulating sample series of the surface elevation via the Monte Carlo approach, coupled with the finite Fourier transform (FFT) technique. This procedure is known to be remarkably efficient for constructing extensive samples with preassigned statistical properties that conform to the assumptions of the underlying theory.

2. SIMULATIONS

We assume that the first-order spectral density S has the Wallops form [Huang *et al.*, 1981], which is given by equation (37) of paper 1 and has the following properties:

$$m_j = m_0 \omega_p^j \left(\frac{m}{4}\right)^{j/4} \Gamma\left(\frac{m-j-1}{4}\right) / \Gamma\left(\frac{m-1}{4}\right) \quad (10)$$

$$v^2 = \Gamma\left(\frac{m-3}{4}\right) \Gamma\left(\frac{m-1}{4}\right) / \Gamma^2\left(\frac{m-2}{4}\right) - 1 \quad (11)$$

$$\kappa^2 = \Gamma\left(\frac{m-5}{4}\right) \Gamma\left(\frac{m-1}{4}\right) / \Gamma^2\left(\frac{m-3}{4}\right) - 1 \quad (12)$$

$$\langle \omega \rangle = \omega_p (m/4)^{1/4} \Gamma\left(\frac{m-2}{4}\right) / \Gamma\left(\frac{m-1}{4}\right) \quad (13)$$

$$\alpha = \langle k \rangle (2m_0)^{1/2} = \langle \omega \rangle^2 (1 + v^2) (2m_0)^{1/2} \quad (14)$$

$$m_0 = \beta g^2 \omega_p^{-4} 4^{(m-5)/4} m^{-(m-1)/4} \Gamma\left(\frac{m-1}{4}\right) \quad (15)$$

We will consider three sets of simulations corresponding to $\alpha = 0.1$, $\alpha = 0.2$, and $\alpha = 0.3$, respectively. For each set, $m = 5, 6, \dots, 20$, so that v varies from a maximum of 0.42 to 0.12, approximately. Because the Wallops shape is defined for $0 < \omega < \infty$ and behaves as ω^{-m} at high frequencies, $\kappa \rightarrow \infty$ at $m = 5$. This result is typical of most theoretical representations of wind wave spectra and must be regarded as an artifact. In practice, empirical spectra are limited to a high-frequency cutoff, say ω^* , such that the spectral area beyond ω^* has essentially negligible contribution to m_0 . In all the cases to be considered here, we set $m_0 = 10m^2$. For a particular α , this enables us to determine ω_p from (13) and β from (15). So far as the contribution of the spectral area over (ω^*, ∞) is concerned, the most critical case corresponds to $\alpha = 0.3$ and $m = 5$, with $\omega_p \approx 0.576$ rad/s and $\beta \approx 0.057$. For $m = 5$ the

spectral area over (ω^*, ∞) is less than $\delta m_0 = \beta g^2 / 4(\omega^*)^4$. Choosing $\omega^* = 2\pi$ rad/s is convenient for FFT and also assures that $\delta m_0 \leq 10^{-3} m^2$. Therefore at least 99.99% of the total spectral mass is accounted for in all cases. As will be shown in section 3, this particular cutoff frequency has essentially no influence on v for all $m \geq 5$ or on κ for $m > 6$ but renders κ bounded at $m = 5$.

In order to utilize the FFT technique in the simulations, we consider the complex process W defined by equation (19) of paper 1 as a function of t at $x = 0$, rewriting it as

$$W(n\Delta) = \sum_{j=0}^{N-1} C_j \exp(i\omega_j n\Delta) \quad n = 0, 1, \dots, N-1 \quad (16)$$

where Δ represents the sampling time interval, $\omega_j = 2\pi j/N\Delta$, and

$$C_j = [2S(\omega_j)\delta\omega]^{1/2} \exp(-i\varepsilon_j) \quad (17)$$

for $j = 1, 2, \dots, (N/2) - 1$ and equals zero otherwise. Here $\delta\omega = 2\pi/N\Delta$, and ε_j denotes the random phases uniformly distributed over $(0, 2\pi)$. The derivative of (16) with respect to $t = n\Delta$ is

$$W_{it}(n\Delta) = - \sum_{j=0}^{N-1} \omega_j^2 C_j \exp(i\omega_j n\Delta) \quad (18)$$

The second-order corrections are defined in terms of η_1 and its Hilbert transform $\hat{\eta}_1$ in the form

$$\eta_{2,s} = \frac{1}{2g} (\hat{\eta}_1 \hat{\eta}_{1,tt} - \eta_1 \eta_{1,tt}) \quad (19)$$

$$\eta_{2,i} = \frac{1}{2g} H[\hat{\eta}_1 \hat{\eta}_{1,tt} - \eta_1 \hat{\eta}_{1,tt}] \quad (20)$$

Since

$$W(n\Delta) = \eta_1(n\Delta) + i\hat{\eta}_1(n\Delta) \quad (21)$$

$$W_{it}(n\Delta) = \eta_{1,tt}(n\Delta) + i\hat{\eta}_{1,tt}(n\Delta) \quad (22)$$

all the quantities required by (19) readily follow from the real and imaginary parts of W and W_{it} via FFT, provided that N is an integral power of 2. To obtain $\eta_{2,i}$, one needs to calculate the Hilbert transform of, say,

$$y = \frac{1}{2g} (\hat{\eta}_1 \eta_{1,tt} - \eta_1 \hat{\eta}_{1,tt}) \quad (23)$$

This is accomplished through a two-step procedure [Tayfun, 1983] whereby we first invert y to compute

$$Y_j = N^{-1} \sum_{n=0}^{N-1} y(n\Delta) \exp(-i\omega_j n\Delta) \quad (24)$$

Then the Hilbert transform of y , i.e., $\eta_{2,i}$, is given by

$$\hat{y}(n\Delta) = \sum_{j=0}^{N-1} G_j Y_j \exp(i\omega_j n\Delta) \quad (25)$$

where $G_j = -i, i$, or 0 , depending on $j < N/2, j > N/2$, or $j = 0$, respectively.

The results to be discussed in the following section were derived from simulations based on a repeated application of the preceding procedure with $N = 2^{13} = 8192$ and $\Delta = 0.5$ s. For each case where α and m are fixed, the estimates of the corresponding statistics and probability densities are obtained from an ensemble of 20 realizations of η_1 , $\eta_{2,s}$, and $\eta_{2,i}$. In other words, the same FFT procedure is repeated 20 times,

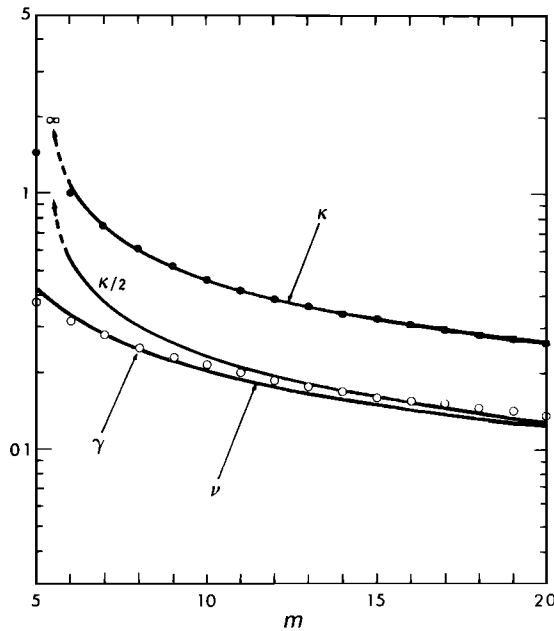


Fig. 1. The parameters ν , κ , and γ . Solid curves show theoretical predictions appropriate to the full Wallops spectrum, solid circles show κ based on the Wallops form with a high-frequency cutoff at $\omega = 2\pi$ rad/s, and open circles show γ .

each time employing a different set of random phases ϵ_j . Therefore σ_η , λ_3 , λ_4 , and all the probability density estimates relevant to η_1 , $\eta_{2,s}$, etc. are in fact derived from a total of $20 \times 8192 = 163,840$ data points for each case.

Recall that λ_3 and λ_4 depend on various mean products of η_1 , $\eta_{2,s}$, and $\eta_{2,l}$. Therefore any sampling or simulation error associated with these mean products will lead to errors in the estimates of λ_3 and λ_4 to be derived from a simulated series of $\eta_1 + \eta_{2,s}$ or $\eta = \eta_1 + \eta_{2,s} + \eta_{2,l}$. The most significant source of such errors is the mean products involving η_1 by itself, namely, the third and fourth moments of η_1 . In theory, $\langle \eta_1^3 \rangle = 0$ and $\langle \eta_1^4 \rangle = 3\sigma_{\eta_1}^4$, so that the skewness and kurtosis of η_1 are both zero. Nevertheless, a simulated series of η_1 will typically yield $\langle \eta_1^3 \rangle = \delta_1 \sigma_{\eta_1}^3$ and $\langle \eta_1^4 \rangle = (3 + \delta_2) \sigma_{\eta_1}^4$, where δ_1 and δ_2 reflect the joint effect of simulation and sampling errors. One can show that these in turn cause errors of the form $\delta_1 (\sigma_{\eta_1} / \sigma_\eta)^3$ and $\delta_2 (\sigma_{\eta_1} / \sigma_\eta)^4$, respectively, in λ_3 and λ_4 computed from a simulated series of $\eta = \eta_1 + \eta_{2,s} + \eta_{2,l}$. In the case of λ_3 and λ_4 corresponding to $\eta_1 + \eta_{2,s}$, the errors

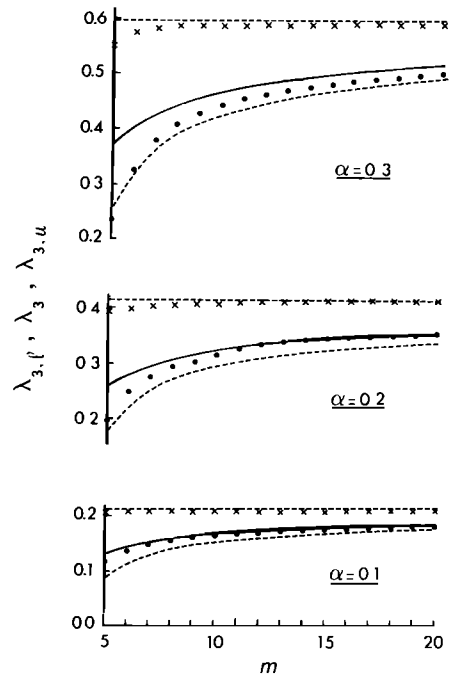


Fig. 3. The skewness coefficient λ_3 and associated bounds. Solid curves show theoretical λ_3 based on the narrow-band model (equation (2)) to $O(\nu)$, dashed curves show the lower bound $\lambda_{3,l}$ given by (6), and dashed lines show the upper bound $\lambda_{3,u}$ given by (8) and appropriate to the narrow-band model to $O(\nu^0)$. Also shown are numerical results derived from simulated series of $\eta_1 + \eta_{2,s}$ (crosses) and $\eta_2 + \eta_{2,s} + \eta_{2,l}$ (solid circles).

have the same forms, except that σ_η is replaced with the rms value of $\eta_1 + \eta_{2,s}$. We found that such errors could be relatively significant in certain cases and accordingly corrected all the estimates λ_3 and λ_4 to be discussed in the following.

3. RESULTS AND COMPARISONS

The theoretical forms of ν and κ based on (11) and (12) and appropriate to the full Wallops spectrum are shown in Figure 1. Also included here is a comparison between ν and $\kappa/2$, which confirms the assertion of paper 1 that $\kappa \approx 2\nu$ when $\nu^2 \ll 1$. We have shown the values of κ corresponding to the Wallops form with the high-frequency cutoff $\omega^* = 2\pi$ with points in the same figure. It is evident that the cutoff modifies the behavior of κ at and near $m = 5$ but has essentially no

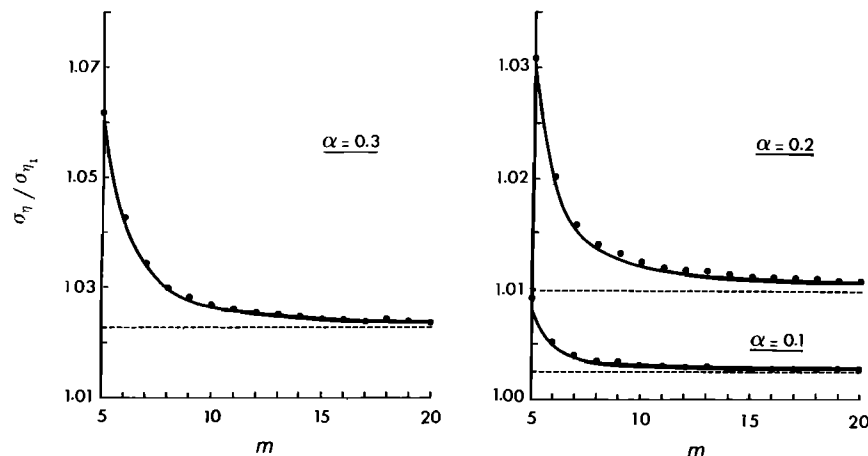


Fig. 2. Comparisons between the exact (solid curves), the narrow-band (dashed lines), and the simulated (solid circles) values of σ_η scaled with $\sigma_{\eta_1} = m_0^{1/2}$.

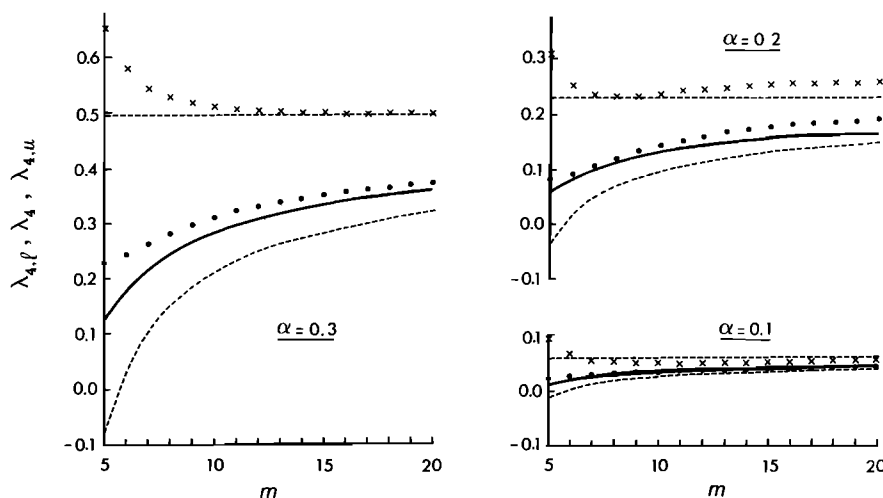


Fig. 4. The coefficient of kurtosis λ_4 and associated bounds. Solid curves show theoretical λ_4 based on the narrow-band model (equation (3)) to $O(v)$, dashed curves show the lower bound $\lambda_{4,l}$ given by (7), and dashed lines show the upper bound $\lambda_{4,u}$ given by (9) and appropriate to the narrow-band model to $O(v^2)$. Also shown are numerical results derived from simulated series of $\eta_1 + \eta_{2,s}$ (crosses) and $\eta_1 + \eta_{2,s} + \eta_{2,i}$ (solid circles).

influence on it for $m > 6$. In the case of v the cutoff has almost no effect, and all values fall on the theoretical curve. Therefore they are not shown separately, for clarity of presentation. In the same figure we also show the parameter γ , which is defined explicitly by equations (53a) and (55) of paper 1 and will be used later to evaluate (2) and (3) here. It is noted that over the range of v considered, the difference between γ and v is less than $\pm 10\%$. Furthermore, the calculations corresponding to $\alpha = 0.1, 0.2$, and 0.3 all gave the same set of identical values of γ shown in Figure 1. Therefore it appears that $\gamma \approx v$ irrespective of α .

The theoretical and simulated results relevant to the variance σ_η scaled with σ_{η_1} are shown in Figure 2. The theoretical results include the predictions based on the exact expression (40) of paper 1 and those of the narrow-band approximation (1) here. Evidently, the simulations compare very favorably with the exact theory, but the discrepancy between the narrow-band predictions and the exact theory is quite substantial, especially at or near $m = 5$ ($v \approx 0.42$). For example, when $\alpha = 0.3$, the narrow-band approximation gives $\sigma_\eta/\sigma_{\eta_1} \approx 1.022$. In other words, the effect of nonlinearities is reflected by an increase of 2.2% in the rms value of the surface elevation. The exact theory predicts an increase of about 6%. Therefore the narrow-band approximation does rather poorly, underestimating the effect of nonlinearities on σ_η by nearly 200%. A similar comparison for $\alpha = 0.1$ and $\alpha = 0.2$ essentially leads to the same conclusion. However, as the spectrum becomes narrow banded, e.g., when $m \geq 10$ ($v \leq 0.20$), the situation improves markedly. When $m = 10$, in particular, the narrow-band approximations suggest that $\sigma_\eta/\sigma_{\eta_1} \approx 1.022, 1.010$, and $1.002(5)$ for $\alpha = 0.3, 0.2$, and 0.1 , respectively. The corresponding values predicted with the exact theory are $\sigma_\eta/\sigma_{\eta_1} \approx 1.027, 1.012$, and 1.003 . In all the three cases now, the narrow-band approximation underestimates the effect of nonlinearities on σ_η by less than 20% relative to the exact theory. For larger values of m the same type of comparison becomes even more favorable. Therefore it would be reasonable to contend that the narrow-band approximation does fairly well in predicting σ_η for $m \geq 10$ ($v \leq 0.20$).

The results on the coefficients of skewness and kurtosis are presented in Figures 3 and 4, respectively. Each figure contains the theoretical predictions derived from the narrow-band

approximation (equation (2) or (3) as appropriate), the corresponding upper and lower bounds, and the simulated results relevant to $\eta_1 + \eta_{2,s}$ and $\eta_1 + \eta_{2,s} + \eta_{2,i}$. Recall that the upper bounds are identical with the predictions of the narrow-band model to $O(v^2)$, which excludes $\eta_{2,i}$. Therefore they are to be compared with the simulations corresponding to $\eta_1 + \eta_{2,s}$. The comparison between the simulated results and the predictions based on the narrow-band approximations is quite favorable, particularly when $\alpha = 0.1$. For $\alpha = 0.2$ and $\alpha = 0.3$ the comparison is still good nearly in all cases when $m \geq 8$ ($v \leq 0.25$), but some discrepancy becomes evident at or near $m = 5$, corresponding to relatively large values of v . In this region the narrow-band approximations tend to overestimate λ_3 and underestimate λ_4 . In comparing the values of λ_3 and λ_4 corresponding to the $\eta_1 + \eta_{2,s}$ and $\eta = \eta_1 + \eta_{2,s} + \eta_{2,i}$ simulations, the opposing effects of $\eta_{2,s}$ and $\eta_{2,i}$ are observed very clearly: the presence of $\eta_{2,i}$ reduces the skewness and kurtosis of η due to $\eta_{2,s}$ in an increasing manner with the larger values of wave steepness and spectral bandwidth. For example, when $\alpha = 0.2-0.3$ and $m \approx 5$ ($v \approx 0.42$), the reduction of λ_3 is nearly 200%, and that of λ_4 is at least 100%.

In order to provide an explicit comparison between the marginal probability densities of $\eta_{2,s}$ and $\eta_{2,i}$ and the Gaussian structure of η_1 , we show in Figure 5 the results derived from simulated series of $\eta_1, \eta_{2,s}$, and $\eta_{2,i}$. Note here that all elevations are normalized with respect to $\sigma_{\eta_1} = m_0^{1/2}$, and $\alpha = 0.3$ as an extreme case. The numerical estimates for the density of η_1 are shown as discrete points (open circles) for $m = 5$ only. As can be expected, these fit the standard Gaussian curve very favorably. Obviously then, the same curve also serves as a basis of reference in all other cases considered. The concentration of the probability masses about the mean level (origin) is indicative of the relative contribution of $\eta_1, \eta_{2,s}$, and $\eta_{2,i}$ to the total surface displacement η . For this particular case, $\eta_{2,s}$ is quite significant and has a symmetrical density that is not much influenced by the spectrum bandwidth. In contrast, the density of $\eta_{2,i}$ is negatively skew and is very much affected by the spectral width. These observations are consistent with the fact that $\eta_{2,s}$ is at least $O(\alpha)$ and has a zero third-order moment and that $\eta_{2,i}$ is at most $O(v)$ and the corresponding third-order moment is negative and $O(v^3)$. Therefore when the spectrum is relatively broad (e.g., $m = 5$

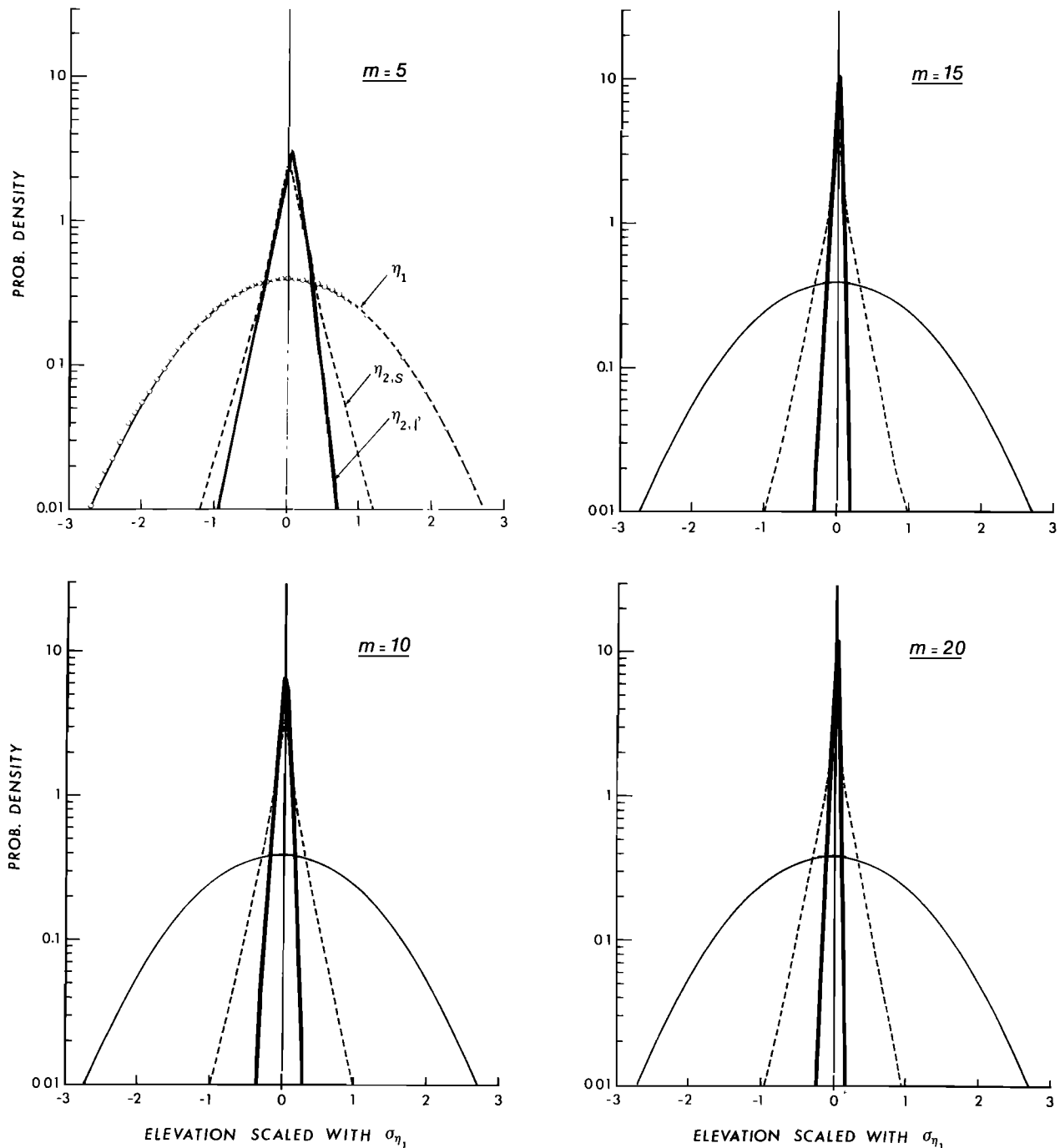


Fig. 5. The comparison between the simulated probability densities of η_1 , $\eta_{2,s}$, and $\eta_{2,l}$ scaled with $\sigma_{\eta_1} = m_0^{1/2}$ ($\alpha = 0.3$).

and $\nu = 0.42$), $\eta_{2,s}$ and $\eta_{2,l}$ have nearly the same order of magnitude, and the corresponding densities look fairly similar. The main discrepancy between the two densities is the negative skewness associated with $\eta_{2,l}$, which simply implies that large modulations of the mean level due to $\eta_{2,l}$ are likely to be more negative than positive. In examining the cases corresponding to $m = 10, 15$, and 20 ($\nu \approx 0.20, 0.15$, and 0.12), we see that when the spectrum becomes increasingly narrow, both the relative importance of and the skewness associated with $\eta_{2,l}$ rapidly diminish, while $\eta_{2,s}$ remains essentially the same.

The results illustrating the individual and combined effects of $\eta_{2,s}$ and $\eta_{2,l}$ on the probability density of the surface elevation η are shown in Figure 6 for $\alpha = 0.3$. The standard Gaussian curve appropriate to η_1/σ_{η_1} is also included in the same

figure for comparison. There are primarily two sets of results shown here, representing the estimates derived from the numerically simulated series of $\eta_1 + \eta_{2,s}$ and $\eta = \eta_1 + \eta_{2,s} + \eta_{2,l}$, each scaled with respect to its own rms value. The comparison between these two sets in essence demonstrates explicitly that when the spectrum is broad, as it is in the case with $m = 5$ ($\nu \approx 0.42$), the skewness and excess associated with the density of η are both relatively small owing to the presence of the long-wave component $\eta_{2,l}$. Toward the other extreme, where $m = 20$ ($\nu \approx 0.12$), $\eta_{2,l}$ gradually disappears from the picture, and the skewness and excess increase in a manner solely determined by $\eta_{2,s}$. Finally, all simulated densities were also compared with the predictions of the Gram-Charlier series by inserting in equation (39) of paper 1 those values of λ_3 and λ_4

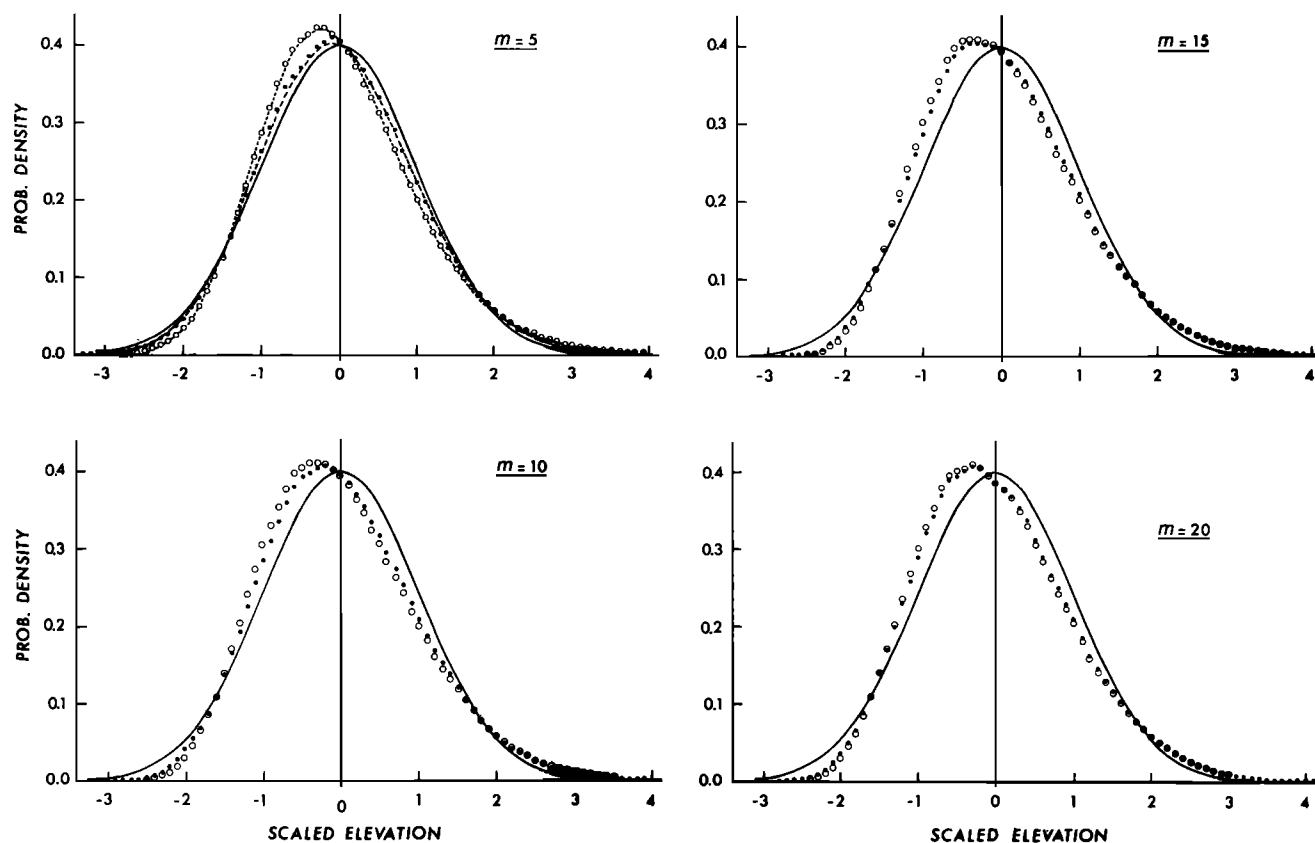


Fig. 6. The comparison between the simulated probability densities corresponding to the linear profile η_1 (solid curves), $\eta_1 + \eta_{2,s}$ (open circles), and $\eta = \eta_1 + \eta_{2,s} + \eta_{2,l}$ (solid circles). The predictions of the Gram-Charlier series are shown for $m = 5$ only (dashed curves). Each elevation is scaled with respect to its own rms value, and $\alpha = 0.3$.

appropriate to each case. A typical example of this comparison is shown in Figure 6 for $m = 5$. Though no comparison is given for the remaining cases $m = 10, 15$, and 20 for clarity of presentation, all the simulated density estimates were in excellent agreement with equation (39) of paper 1.

4. CONCLUDING REMARKS

The predictions based on the narrow-band approximation to $O(v)$ compare very favorably with those derived from the simulations of the second-order "exact" theory, especially for small values of wave steepness and narrow-band spectra. Assuming that a particular sea state can be modeled with the Wallops spectral form, it appears that the proposed model is capable of presenting the main principles implied by the exact theory in a simple manner and that it provides fairly accurate quantitative results when $m \geq 10$ ($v \leq 0.20$).

The data presented by Huang *et al.* [1981] and Liu [1983] indicate that $5 < m < 11$ for a number of actual wind wave spectra. This probably gives us a reasonable estimate on the likely range of m values that would be expected for wind waves within a generation area. On this basis and because we also ignored wave directionality and surface stresses, the quantitative accuracy of the model within the generation area is open to question. However, as waves propagate out of the generation area, not only is their spectral form likely to become progressively more narrow banded, but also their directional spread will tend to be narrow beamed. Therefore we expect that the narrow-band representation would be more appropriate to such cases.

We restricted attention to deep water waves only and there-

fore ignored the effects of finite water depths on the probability structure and the key statistics of the surface elevation. In finite water the mathematics becomes considerably difficult to handle in the same systematic manner as the one demonstrated in paper 1, and a primarily numerical approach may have to be employed. Past studies elaborate different aspects of the overall problem and provide us with partial answers. Some of these appear to be contrary to one another as well as to certain implications of the present study. For example, Tick's [1961] results suggest that spectral amplitudes typically associated with the long-wave modulation are enhanced substantially because of shoaling as waves advance toward shallower depths. In view of this, the present results would imply that the surface skewness should decrease as the water depth decreases. This would certainly agree with the conclusions of Sharma and Dean [1979]. However, it is less certain what happens when the problem is treated under a more realistic setting that would include wave refraction and its consequences on directional spectra. For example, a limited number of results derived by Tuah and Hudspeth [1985] indicate that the skewness is always positive and increases considerably as the water depth decreases. If so, the density of surface elevations of shallow water wind waves would typically display a highly asymmetric form, in agreement with some observations [Bitner, 1980; Huang *et al.*, 1983]. In retrospect, it is evident that the general problem is of considerable theoretical and practical interest and requires further research.

The random phase simulation scheme is one of two principal approaches presently available where the simulation consists of summing a finite number N of Fourier compo-

nents. The alternative is a random coefficient scheme in which the component amplitudes represent independent Gaussian variates. For the former scheme, the underlying probability density becomes asymptotically Gaussian as $N \rightarrow \infty$, whereas for the latter it is already Gaussian for any N . A recent article by Tucker *et al.* [1984] presents a critical review of both schemes and contends that the random phase approach does not correctly simulate wave characteristics for a Gaussian sea state but that the random coefficient scheme does. This contention is demonstrated to some extent with reference to several case studies on wave group characteristics and with a specific simulation example, in which N is 900 for the random coefficients and 100 for the random phase scheme. It is true that with the random phase scheme, problems and inaccuracies can arise in simulating wave group characteristics if N is relatively small. Nonetheless, it is also known that when N is sufficiently large (as it is in the present case), both schemes are essentially identical and yield the same results [Elgar *et al.*, 1984]. Evidently, this is confirmed further here by the fact that the simulated results compare very favorably with theory when they are expected to

Acknowledgments. This study, like paper 1, was supported by Kuwait Foundation for the Advancement of Sciences under grant 84-09-03. The helpful comments of the reviewers are gratefully acknowledged.

REFERENCES

- Bitner, E. M., Nonlinear effects of the statistical model of shallow-water wind waves, *Appl. Ocean Res.*, 2(2), 63-73, 1980.
- Elgar, S., R. T. Guza, and R. J. Seymour, Groups of waves in shallow water, *J. Geophys. Res.*, 89(C9), 3623-3634, 1984.
- Huang, N. E., S. R. Long, C. C. Tung, Y. Yuen, and L. F. Bliven, A unified two-parameter wave spectral model for a general sea state, *J. Fluid Mech.*, 112, 203-224, 1981.
- Huang, N. E., S. R. Long, C. C. Tung, Y. Yuen, and L. F. Bliven, A non-Gaussian statistical model for surface elevation of nonlinear random wave fields, *J. Geophys. Res.*, 88, 7597-7606, 1983.
- Liu, P. C., A representation for the frequency spectrum of wind-generated waves, *Ocean Eng.*, 10(6), 429-441, 1983.
- Longuet-Higgins, M. S., The effect of nonlinearities on statistical distributions in the theory of sea waves, *J. Fluid Mech.*, 17, 459-480, 1963.
- Sharma, J. N., and R. G. Dean, Development and evaluation of a procedure for simulating a random directional second order sea surface and associated wave forces, *Ocean Eng. Tech. Rep. 20*, Dep. of Civ. Eng., Univ. of Del., Newark, 1979.
- Tayfun, M. A., Frequency analysis of wave heights based on wave envelope, *J. Geophys. Res.*, 88(C12), 7573-7587, 1983.
- Tayfun, M. A., On narrow-band representation of ocean waves, 1, Theory, *J. Geophys. Res.*, this issue.
- Tick, L. J., Nonlinear probability models of ocean waves, in *Ocean Wave Spectra*, pp. 163-171, Prentice-Hall, Englewood Cliffs, N. J., 1961.
- Tuah, H., and R. T. Hudspeth, Finite water depth effects on nonlinear waves, *J. Waterw. Port Coastal Ocean Div. Am. Soc. Civ. Eng.*, 111(2), 401-416, 1985.
- Tucker, M. J., P. G. Challenor, and D. J. T. Carter, Numerical simulation of a random sea: A common error and its effect upon wave group statistics, *Appl. Ocean Res.*, 6, 118-222, 1984.

M. A. Tayfun, Civil Engineering Department, College of Engineering and Petroleum, Kuwait University, P.O. Box 5969, Kuwait, 13060.

(Received July 22, 1985;
accepted December 23, 1985.)